



**HAL**  
open science

## Nickel catalyst faceting in plasma-enhanced direct current chemical vapor deposition of carbon nanofibers

Z. B. He, Jean-Luc Maurice, C. S. Lee, C. S. Cojocaru, D. Pribat

### ► To cite this version:

Z. B. He, Jean-Luc Maurice, C. S. Lee, C. S. Cojocaru, D. Pribat. Nickel catalyst faceting in plasma-enhanced direct current chemical vapor deposition of carbon nanofibers. *Arabian Journal for Science and Engineering*, 2010, 35 (1C), pp.19. hal-00525291

**HAL Id: hal-00525291**

**<https://polytechnique.hal.science/hal-00525291>**

Submitted on 12 Oct 2010

**HAL** is a multi-disciplinary open access archive for the deposit and dissemination of scientific research documents, whether they are published or not. The documents may come from teaching and research institutions in France or abroad, or from public or private research centers.

L'archive ouverte pluridisciplinaire **HAL**, est destinée au dépôt et à la diffusion de documents scientifiques de niveau recherche, publiés ou non, émanant des établissements d'enseignement et de recherche français ou étrangers, des laboratoires publics ou privés.

# Nickel catalyst faceting in plasma-enhanced direct current chemical vapor deposition of carbon nanofibers

Z. B. He,<sup>a</sup> J.-L. Maurice,<sup>a,\*</sup> C. S. Lee,<sup>a</sup> D. Pribat,<sup>b</sup> and C. S. Cojocaru<sup>a</sup>

<sup>a</sup>Laboratoire de Physique des Interfaces et Couches Minces, LPICM, UMR 7647, École Polytechnique-CNRS, Route de Saclay, 91128 Palaiseau Cedex, France

<sup>b</sup>Departement of Energy Science, Sungkyunkwan University Suwon 440-746, Korea

Vertically aligned multi-walled carbon nanofibers (CNFs) were grown by plasma-enhanced chemical vapor deposition with Ni catalysts on the top of nanofibers. Transmission electron microscopy was used to study the morphology and crystallography of Ni catalysts, which are essential for the nucleation and growth of CNFs. A model for the faceted shape of Ni catalytic particles is proposed. It is shown that the exposed polyhedral surfaces of Ni catalytic particles for vertically aligned CNFs are composed of {111}, {110}, and {100}, a faceting that appears to be characteristic of the growth atmosphere.

**Key words:** carbon nanofibers (CNFs), PECVD, Ni catalysts, Ni faceting, TEM

---

\* Corresponding author: Tel: +33 1 6933 4344, Fax: +33 01 69 33 43 33, E-mail: jean-luc.maurice@polytechnique.edu

## I. INTRODUCTION

Since the discovery of carbon nanotubes (CNTs) in 1991 by Iijima [1], CNTs as well as carbon nanofibers (CNFs), especially their ordered arrays, have attracted a great deal of attention, not only because of theoretical interest, but also for their superior properties such as high thermal conductivity, excellent electron emission properties and wonderful electron transport with potential commercial applications in electronics, mechanics, chemistry and biochemistry [2-8]. A multi-walled CNT consists of concentric cylinders of rolled graphene sheets, whereas a CNF is made of stacked cone-shaped graphite planes. The primary difference between CNTs and CNFs is the angle ( $\theta$ ) between the graphite basal planes and the tube axis ( $\theta = 0^\circ$  for CNTs;  $\theta \neq 0^\circ$  for CNFs), which can be controlled by, *e.g.*, the amount of hydrogen in the growth atmosphere [9, 10]. Increasing hydrogen concentration would tend to tilt the basal planes away from the cylinder axis to form CNFs [11]; while on the contrary, suppressing hydrogen would allow carbon to deposit in the closed forms of shells or CNTs [12].

High temperature preparation techniques such as arc discharge or laser ablation were first used to produce CNTs or CNFs and were then replaced by low temperature chemical vapor deposition (CVD) techniques ( $< 800^\circ\text{C}$ ), since the orientation, alignment and density of CNTs can be precisely controlled in the latter [12,13]. Transition metal nanoparticles, primarily Fe, Co or Ni, are typical catalysts for the growth of CNTs or CNFs using CVD [13-16, 17, 18]. The growth mechanism of the catalytic growth of CNFs have been discussed in some classic works by Baker et al.[18, 19]. In the case of Fe and Ni thin films, forming nano-sized particles by high-temperature de-wetting, it was shown that the diameter of the CNTs strongly depended on the starting thickness of catalyst layer [20]. Correlations between the size of metal catalyst nanoparticles and carbon nanotube growth have been found and discussed [21]. Besides, the initial stages of the growth of vertically aligned carbon nanofibers

were studied by using both scanning and transmission electron microscopy (TEM) [22]. Moreover, Helveg *et al.* observed directly the formation of CNFs catalyzed by Ni nanoparticles using time resolved, high-resolution *in situ* TEM [23]. The influence of the composition and the morphology of the catalyst nanoparticles on the growth of CNTs by CVD are summarized in a review paper [24]. However, the crystallography of catalysts has only been the object of few experimental studies [25, 26], and the correlations between the catalytically active surfaces of transition metal catalysts and CNFs are still not clear. In this study, we will focus on a TEM investigation of the crystallography of Ni catalysts for the vertical growth of CNFs, which were synthesized by direct current (dc) plasma-enhanced CVD (dc PECVD) in an atmosphere composed of isopropyl alcohol ( $\text{CH}_3\text{CH}(\text{OH})\text{CH}_3$ ) and water ( $\text{H}_2\text{O}$ ). A three-dimensional (3D) model at the atomic scale of a faceted shape of Ni catalytic nanoparticle is proposed based on the bright-field TEM image observations. The top surface of Ni catalysts is found indeed to be faceted like a Wulff polyhedron, while observations of similar catalysts in other growth conditions exhibited more rounded features and a  $\{110\}$  preferential faceting [26], or flat and exclusively  $\{111\}$  facets [25]. Finally, the Ni particle faceting is discussed as a consequence of the growth atmosphere and of the way nucleation and early stages of growth take place.

## II. EXPERIMENTS

Vertically aligned CNF arrays were grown from Ni catalysts originating from thin films with different thicknesses. We used bare Si as substrate, and growth was performed by dc PECVD at 600 °C for 85 minutes or 650 °C for 20 minutes, at a pressure of 2 mbars. A mixture of water vapor and isopropyl alcohol with a flow rate of 7.5 sccm and 4.5 sccm, respectively, was used as the reactive gas sources. The gas flows were precisely controlled to get a C/H ratio of  $\sim 0.26$  which avoided the generation of amorphous carbon on the surface of

catalysts. In order to obtain well aligned CNFs, the applied voltage between anode and cathode in the chamber was kept constant at 500 V, and with a current intensity of 0.2 A. The extraction voltage and the current were slowly increased up to the optimum conditions at the beginning of the growth process. At the end of the growth process, the chamber was totally pumped out and cooled down. Cooling took around 30 minutes without any gas flow. The length of CNFs was controlled by the growth time and their diameter by the thickness of the starting Ni film. The CNFs were observed using a Hitachi S-4800 FE-scanning electron microscope (SEM) with 25 kV accelerating voltage. The microstructures of CNFs and Ni catalysts were studied by TEM using a Philips CM 30 working at 300 kV, and a Topcon 002B working at 120 kV.

### III. RESULTS

Figure 1 shows typical SEM images of top-type CNFs, which are well aligned and oriented perpendicular to the Si substrate. The CNFs were grown at 600 °C for 85 min, using two thicknesses of Ni (50 nm in (a) and 20 nm in (b)), on a bare Si substrate. Each CNF has a uniform diameter with one Ni particle on the top. As in other works, the present Ni-catalyst particles on the top of CNFs have inversed water drop shape, elongated along the CNFs. In contrast to several other observations, they exhibit clearly defined facets.

#### Figure 1

Different morphologies of Ni particles for the top-type vertically aligned CNFs were found. Figure 2 (a) is a typical low magnification TEM image of a bunch of CNFs with Ni particles on their tops. The diameter of the bottom of the CNFs is large because several CNFs with different lengths grew together. SEM images recorded at different growth stages (not shown) indicate that the size of Ni particles on the top of CNFs is smaller than that at the

initial stage of the growth of CNFs. Hence we deduce that a bundle of CNFs might nucleate from the same large Ni particle at the initial stage, and then grow to different lengths perhaps due to different carbon concentrations in the Ni catalysts, because the gas phase is cleaner close to the substrate, the growth nutrients having been consumed by the longer CNFs. Figure 2(b) is a bright-field TEM micrograph taken along the [1-10] zone axis of the Ni particle. The spearhead-like Ni particle exhibits two {111} carbon-free top surfaces having a mirror symmetry with respect to the (001) plane. A thin layer of crystallized NiO, caused by electron irradiation in the microscope, shows a light contrast on the top of the spearhead.

### Figure 2

Figure 2 (c) and (d) reveal Ni particles with {111} twin planes nearly perpendicular to or parallel to the axes of CNFs, respectively. The crystallographic planes of the top surfaces of the Ni particle in (c) are determined as {111}, the same as in (b), whereas the top surfaces of the Ni particle in (d) consist of some different planes besides {111}, which can be analyzed by the angles between the top surfaces and the obvious {111} twin faces since the angle between two {111} cubic planes is  $70.53^\circ$  (or  $109.47^\circ$ ). In addition to the straight twin boundaries in the Ni particle, more general grain boundaries (or tilted twin boundaries) between two crystal variants in one Ni catalyst were also found, as seen in Fig. 2(e). However, the intersections of those boundaries with the particle surface do not create visible surface step or discontinuity. And indeed, the graphene layers of CNFs are not affected by the grain boundaries. Sometimes, the Ni particle can be bent and hence change its growth orientation [Fig. 2(f)]. As a result, the corresponding orientation of CNFs at its top is deviated from the initial one. In correlation with that bending, the thickness of the graphite layers on both side surfaces of the top of CNFs in Fig. 2(f) is different. In general, although the morphologies of Ni particles are different, there are some common characteristics: (1), the shape of the

catalysts for the growth of CNFs prefer to be pear like (also known as water drop like or tear drop like); (2), each Ni particle consists of two parts: head (free from graphene coverage) and body (covered by graphene layers); (3), the head presents low-index facets while the body does not; (4), the size of the head and the tail of the water drop like Ni catalysts determine the external diameter and the one of the inner hole of CNFs, respectively; (5), neither twins nor grain boundaries affect the growth of CNFs.

### Figure 3

All the observed Ni particles for vertically aligned CNFs are faceted, with facets corresponding to low-index planes, particularly  $\{111\}$  (Fig. 2). This result is different from other observations [26], which we will discuss in the next section. In order to more precisely analyze the crystallographic surfaces of Ni, we tilted one Ni particle along two mutually perpendicular directions to get three images [Fig. 3]. Figure 3(a) shows the projection of the Ni particle along  $[-100]$ . The top surfaces of Ni particle consist of low index (010), (001) and (011) planes which are showing edge-on as straight lines. The Ni particle was tilted by  $\sim 6^\circ$  from the horizontal, and the growth direction is thus determined as  $[011]$  from the relationship between the selected area electron diffraction pattern (EDP) and the corresponding bright-field image (after correcting for the instrumental rotation). When we tilt the sample about the axial direction of the CNF by  $\sim 35^\circ$  to the  $[-2-11]$  zone axis [Fig. 3(b)], the morphology of the top surfaces of the Ni particle changes: the corresponding projected top surfaces from this direction are (113), (011) and  $(-131)$ . But the crystallographic (011) plane remains the same as that in (a) since it is normal to the axis of the CNF. Furthermore, we tilted the sample from  $[-2-11]$  in (b) to  $[-1-10]$  in (d) by  $\sim 30^\circ$ , namely  $\sim 45^\circ$  from  $[-100]$  in (a). The top facets of Ni in Fig. 3 are mainly composed of low-index  $(1-1-1)$ , (011), and (001) planes. The (001) facet is visible in both (a) and (d). It is not strange that the length of Ni particle in (d) becomes shorter

than that in (a) because it is just a projected image from (a). It should be mentioned that one should be very careful when determining the growth direction of one dimensional nano materials as the sample may be tilted to a relatively large angle from the horizontal, e.g., the schematic illustration in Fig. 3 (c). By combining the information of the experimental results in Fig. 3, we propose a primary 3D structural model for the faceted shape of the Ni particle (Fig. 4). Figure 4 (a), (b) and (d) are the structural projections of the model from  $[-100]$ ,  $[-2-11]$  and  $[-1-10]$  directions, which are consistent with the correlated experimental images in Fig. 3, respectively. The exposed top surfaces of Ni are linked by yellow lines, and the side surfaces are marked by blue lines. In order to expose the topography of the top surfaces of the structural model clearly, we use different colors to display the first three layers in the 3D model in Fig. 4(c). Note that the same layer was highlighted by the same color in Fig. 4 (a). The foremost plane is (011), the stacking sequence of which controls the growth direction of the Ni particle. It is interesting to note that the carbon-free (1-1-1) plane is larger than the others.

These low-index facet orientations correspond to low surface energy; however, the presence of sharp edges gives a shape which is not yet that of a Wulff polyhedron [27], which is to say that the top surface is still far from thermal equilibrium.

#### Figure 4

## IV. DISCUSSION

The surfaces of Ni catalysts are very significant for the nucleation and growth of CNFs since they play a key role in (1) propan-2-ol dissociation, (2) surface diffusion of carbon atoms, and (3) segregation and crystallization of the latter. Audier *et al.* showed that carbon-free planes of catalytic transition metal alloys for CNTs were dependent on the crystal structure of body-centred or face-centred cubic (fcc) [25]. These authors also concluded that



in the case of fcc metals, only {111} facets could be observed. They used catalytic disproportionation of CO at  $P = 1$  atm and  $450\text{ }^{\circ}\text{C} < T < 650\text{ }^{\circ}\text{C}$  [25]. In contrast, Kuang *et al.* found that the {110} orientation of Ni particles was preferred as the top surfaces [26]. These authors used a mix based on CH<sub>4</sub>, in a hot-wire PE-CVD equipment, at  $P = 3$  kPa, and  $T = 700\text{ }^{\circ}\text{C}$ . Yang and Chen [28] reported that {110} faces were catalytically active for the dissociation of CH<sub>4</sub>, while {111} was not. Here, we found not only {110} planes as in Ref. 26, and {111} as in Ref. 25, but also other low index crystallographic planes such as {100}. Such kind of polyhedral top surfaces reminds one of the equilibrium shapes of Wulff polyhedra, which indicates the tendency of minimizing surface energy by exposing low-index facets. On the contrary, side surfaces mainly consist of high-index planes: They are higher energy surfaces, including a high density of atomic steps, perhaps playing an important catalytic action in the crystallization of graphene layers [23]. Our observations are somewhat different from the conclusions of Yang and Chen [28], who had shown that, on the one hand, {100} and {110} surfaces were the most active in the decomposition of CH<sub>4</sub> at 700 °C, and, on the other hand, {111} and {311} were the most efficient for the epitaxy of the graphene layers. At least three conditions, however, differ between our work and that of Yang and Chen [28]: (1) theirs was at a pressure of 1 atmosphere while ours is at 1 mbar, (2) their atmosphere was pure CH<sub>4</sub>, while our atmosphere is composed of a mixture of water vapor and isopropyl alcohol, and (3), theirs was standard CVD, while ours is dc PECVD. Thus the dynamic equilibria that establish at surfaces during growth should be different in the two cases.

### Figure 5

The increasing number of graphene layers from the head to the foot of Ni particles may explain why the Ni particles have a pear-like shape with a large size at the head, and a small size at the foot. Figure 5(a) is a high resolution electron microscope (HREM) image showing

the change of the number of graphene layers at the top of Ni catalyst. There are only three graphene layers at the highest side surface of Ni producing a relative small compressive stress on the Ni particle, but the number of graphene layers increases along an arrow direction to cause a relatively large pressure to compress the Ni particle to a smaller diameter. As a result, the Ni catalyst adopts a pear-like shape with a big size at the position covered with few graphene layers, and elongates along the axis of CNFs. The compressive stress from graphene layers of CNTs could even extract Fe<sub>3</sub>C along the tubes due to a stress as large as 40 gigapascals [29]. Graphene layers of CNFs are always parallel to the side surface of Ni catalysts (Fig. 5b) and, hence the  $\theta$  angle is dictated directly by the slope of the side surfaces of the polyhedral Ni catalyst. Nolan *et al.* have shown that the  $\theta$  angle could be increased by increasing hydrogen in the chamber because hydrogen was able to saturate the additional surface dangling bonds introduced by the increase of  $\theta$  [9, 10]. With the new cone-shaped graphene layers formed layer by layer from the side surfaces of Ni particle, the CNF becomes longer and longer along the axis of the elongated Ni particle (Fig. 6).

### Figure 6

Normally, it is difficult for graphene layers to grow beyond the top of the Ni particle since the edges of graphene layers are easily etched by energetic ions and highly reactive neutral species such as atomic hydrogen, as explained in Ref. 30 (red “x” in Fig. 5a). It seems that the conical Ni particles at the top of CNFs act as moulds to produce cone-shaped layer structure. Therefore, the inner and external diameters of the top-type CNFs are determined by the size of the tail and head of the elongated Ni particle, respectively.

## **V. CONCLUSIONS**

Vertically aligned CNFs were grown by the tip-growth mechanism, using dc PECVD at low temperatures and  $\text{H}_2\text{O} + \text{CH}_3\text{CH}(\text{OH})\text{CH}_3$  gas mixtures. The exposed surfaces of the Ni particles at the growth front are a combination of low index planes such as  $\{111\}$ ,  $\{110\}$ , and  $\{100\}$ , as in a Wulff polyhedron, rather than a unique type of facet such as  $\{111\}$ [25] or  $\{110\}$  [26]. Planar defects such as  $\{111\}$  twins with twin boundaries parallel to or almost perpendicular to the CNT were found in the Ni catalysts. Although different faceted shapes of the Ni particles are found, the cone-shaped graphene layers of CNFs are always parallel to the side surfaces of the Ni particles, which in turn have high indices. The synthesis mechanism of the CNF involves nucleation and growth of each graphene layer on the side walls of the Ni particle, followed by their repelling by the next nucleated layer. The resulting structure is a stack of parallel graphene layers “molded” on the side wall of the conical Ni particle and consequently oriented at an angle with respect to the CNF axis. The inner and external diameters of the CNFs are determined by, respectively, the diameters of the tails and of the heads of the elongated Ni catalyst particles.

## **ACKNOWLEDGEMENTS**

This work has been supported by the Region Ile-de-France in the framework of C’Nano IdF. C’Nano IdF is the nanoscience competence center of Paris Region, supported by CNRS, CEA, MESR and Region Ile-de-France. It was also partially funded by the European Community project OPTHER (FP 7) and the French ANR project SIMS. One of authors (Z.B. He) thanks Dr. G. Rizza and F. Attouchi at Laboratoire des Solides Irradiés, Ecole Polytechnique, France for useful discussions. Thanks are also due to Dr. J.-E. Bourée for careful reading of the manuscript.

## References

- [1] S. Iijima, "Helical microtubules of graphitic carbon", *Nature*, **354**(1991), pp. 56-58.
- [2] R. Martel, T. Schmidt, H. R. Shea, T. Hertel, and Ph. Avouris, "Single- and multi-wall carbon nanotube field-effect transistors", *Appl. Phys. Lett.* **73**(1998), pp. 2447-2449.
- [3] Z. F. Ren, Z. P. Huang, J. W. Xu, J. H. Wang, P. Bush, M. P. Siegal, and P. N. Provencio, "Synthesis of Large Arrays of Well-Aligned Carbon Nanotubes on Glass" *Science*, **282**(1998), pp.1105-1107.
- [4] M. S. Dresselhaus, G. Dresselhaus, and P. Avouris, *Carbon Nanotubes: Synthesis, Structure, Properties and Applications*, Springer, Berlin (2001).
- [5] J. Robertson, "Realistic applications of CNTs", *Mat. Today*, **7**(2004), pp. 46-52.
- [6] D. Pribat, C. S. Cojocaru, M. Gowtham, L. Eude, P. Bondavalli, P. Legagneux, "Carbon nanotubes and semiconductor nanowires for active-matrix backplanes", *J. SID*, **15**(2007), pp. 595-600.
- [7] E. Bichoutskaia<sup>1</sup>, A. M. Popov, and Y. E. Lozovik, "Nanotube-based data storage devices", *Mat. Today*, **11**(2008), pp. 38-43.
- [8] T. Y. Tsai, C. Y. Lee, N. H. Tai, and W. H. Tuan, "Transfer of patterned vertically aligned carbon nanotubes onto plastic substrates for flexible electronics and field emission devices", *Appl. Phys. Lett.*, **95**(2009), pp. 013107 (1-3).
- [9] P. E. Nolan, M. J. Schabel, D. C. Lynch, and A. H. Cutler, "Hydrogen control of carbon deposit morphology", *Carbon*, **33**(1995), pp.79-85.
- [10] P. E. Nolan, D. C. Lynch, and A. H. Cutler, "Carbon Deposition and Hydrocarbon Formation on Group VIII Metal Catalysts", *J. Phys. Chem. B*, **102**(1998), pp. 4165-4175.
- [11] H. Murayama, and T. Maeda, "A novel form of filamentous graphite", *Nature*, **345**(1990), pp. 791-793.

- [12] W.Z. Li, S.S. Xie, L.X. Qian, B.H. Chang, B.S. Zou, W.Y. Zhou, R.A. Zhao, G. Wang, “Large-Scale Synthesis of Aligned Carbon Nanotubes”, *Science*, **274**(1996), pp. 1701-1703.
- [13] M. Meyyappan, L. Delzeit, A. Cassell and D. Hash, “Carbon nanotube growth by PECVD: a review”, *Plasma Sources Sci. Technol.*, **12**(2003), pp. 205-216.
- [14] V. I. Merkulov, D. H. Lowndes, Y. Y. Wei, G. Eres, and E. Voelkl, “Patterned growth of individual and multiple vertically aligned carbon nanofibers”, *Appl. Phys. Lett.*, **76**(2000), pp. 3555 (1-3).
- [15] M. Chhowalla, K. B. K. Teo, C. Ducati, N. L. Rupesinghe, G. A. J. Amaratunga, A. C. Ferrari, D. Roy, J. Robertson, and W. I. Milne, “Growth process conditions of vertically aligned carbon nanotubes using plasma enhanced chemical vapor deposition”, *J. Appl. Phys.* **90**(2001), pp.5308 (1-10).
- [16] C. Bower, O. Zhou, W. Zhu, D. J. Werder, S. Jin, “Nucleation and growth of carbon nanotubes by microwave plasma chemical vapor deposition”, *Appl. Phys. Lett.*, **77**(2000), pp. 2767 (1-3).
- [17] R. T. K. Baker, J. J. Chludzinski, J.R., Dudash, and A. J. Simoens, “The formation of filamentous carbon from decomposition of acetylene over vanadium and molybdenum”, *Carbon*, **21**(1983), pp. 463-468.
- [18] R. T. K. Baker, M. A. Barber, P. S. Harris, F. S. Feates and R. J. Waite, “Nucleation and growth of carbon deposits from the nickel catalyzed decomposition of acetylene”, *J. Catalysis*, **26**(1972), pp. 51-62.
- [19] R. T. K. Baker, J. Chludzinski, and R. D. Sherwood, “A comparison of the catalytic influence of nickel, iron and nickel-iron on the gasification of graphite in various gaseous environments”, *Carbon*, **23**(1985), pp. 245-254.

- [20] Y. Y. Wei, G. Eres, V. I. Merkulov, and D. H. Lowndes, "Effect of catalyst film thickness on carbon nanotube growth by selective area chemical vapor deposition", *Appl. Phys. Lett.*, **78**(2001), 1394 (1-3).
- [21] E. F. Kukovitsky, S. G. L'vov, N.A. Sainov, V.A. Shustov, and L. A. Chernozatonskii, "Correlation between metal catalyst particle size and carbon nanotube growth", *Chem. Phys. Lett.*, **355**(2002), pp. 497-503.
- [22] H. Cui, X. Yang, M. L. Simpson, D. H. Lowndes, and M. Varela, "Initial growth of vertically aligned carbon nanofibers", *Appl. Phys. Lett.*, **84**(2004), pp. 4077 (1-3).
- [23] S. Helveg, C. Lopez-Cartes, J. Sehested, P. L. Hansen, B. S. Clausen, .R. Rostrup-Nielsen, F. Abild-Pedersen, and J. K. Nørskov, "Atomic-scale imaging of carbon nanofibre growth", *Nature*, **427**(2004), pp. 426-429.
- [24] A.-C. Dupuis, "The catalyst in the CCVD of carbon nanotubes—a review", *Progr. Mat. Sci.*, **50**(2005), 929-961.
- [25] M. Audier, A. Oberlin, and M. Coulon, "Crystallographic orientations of catalytic particles in filamentous carbon; Case of simple conical particles", *J. Cryst. Growth*, **55**(1981), pp. 549-556.
- [26] M. H. Kuang, Z. L. Wang, X. D. Bai, J. D. Guo, and E. G. Wang, "Catalytically active nickel {110} surfaces in growth of carbon tubular structures", *Appl. Phys. Lett.*, **76**(2000), pp. 1255 (1-3).
- [27] For a demonstration of Wulf theorem, see e.g. P. Muller and R. Kern, *Surf. Sci.* , **457**(2000), pp. 229.
- [28] R. T. Yang and J. P. Chen, "Mechanism of carbon filament growth on metal catalysts", *J. Catal.*, **115**(1989), pp. 52-64.

[29] L. Sun, F. Banhart, A. V. Krasheninnikov, J. A. Rodriguez-Manzo, M. Terrones, P. M. Ajayan, “Carbon nanotubes as high-pressure cylinders and nanoextruders”, *Science*, **312** (2006), pp. 1199-1202.

[30] C. S. Cojocaru, A. Senger, and F. Le Normand, “A Nucleation and Growth Model of Vertically-Oriented Carbon Nanofibers or Nanotubes by Plasma-Enhanced Catalytic Chemical Vapor Deposition”, *J. Nanosci. Nanotechnol.*, **6**(2006), pp. 1331(1-8).



## Figure captions

Fig. 1. SEM images of vertically aligned top-type CNFs grown on different thicknesses of Ni catalytic layers: (a) 50 nm; (b) 20 nm. The averaged length of CNFs in Fig. 1(a) is around 5  $\mu\text{m}$ , which can be increased or reduced with the growth time. The Ni particles have facets, and the average size increases with the thickness of the Ni layer.

Fig. 2. (a) Low magnification TEM image of a bunch of CNFs with Ni catalyst particles on top (marked by black arrowheads). The longest CNF is about 4  $\mu\text{m}$ . (b)-(f) TEM bright-field images of Ni particles on the top of CNFs. Defects such as twins in (c) and (d) as well as grain boundaries in (e) are found in the Ni catalysts, but have few effects on the growth of CNFs. Many of the exposed surfaces of Ni have  $\{111\}$  indices.

Fig. 3. (a), (b) and (d) A series of TEM bright-field images of the same Ni particle taken at the same magnification, but viewed along different zone axes: (a)  $[-100]$ ; (b)  $[-2-11]$ ; and (d)  $[-1-10]$ ; (c) Schematics of the tilted angle from (a) to (d). The growth direction of the CNF is determined as  $[011]$  from (a). Note that if the CNF is tilted by a large angle from the horizontal, the growth direction deduced from the corresponding EDP is not the real value, e.g.  $[-112]$  in (c) and (d).

Fig. 4. A model for the faceted Ni particle of Fig. 3. (a), (b), and (d): Projections of the 3D model in (c) along (a)  $[-100]$ , (b)  $[-2-11]$ , and (c)  $[-1-10]$ , which correspond to the experimental images in Fig. 3, respectively.

Fig. 5. HREM images of Ni and graphene layers. (a) The head of Ni particle. Note that the edges of the graphene layers are found in the external sides of CNF, as marked by black arrowheads. The number of graphene layers at the highest side surfaces is three and increasing along the direction of a black arrow. (b) The foot of Ni particle. Graphene layers are parallel to the side surface of Ni.

Fig. 6. Schematics of the growth of top-type CNFs. Forbidden growth directions, marked by a red “x”, are mainly caused by the etching of impinging highly reactive neutral species. Note that the side surface acts as a mould for the growth of CNFs (from (a) to (b)).

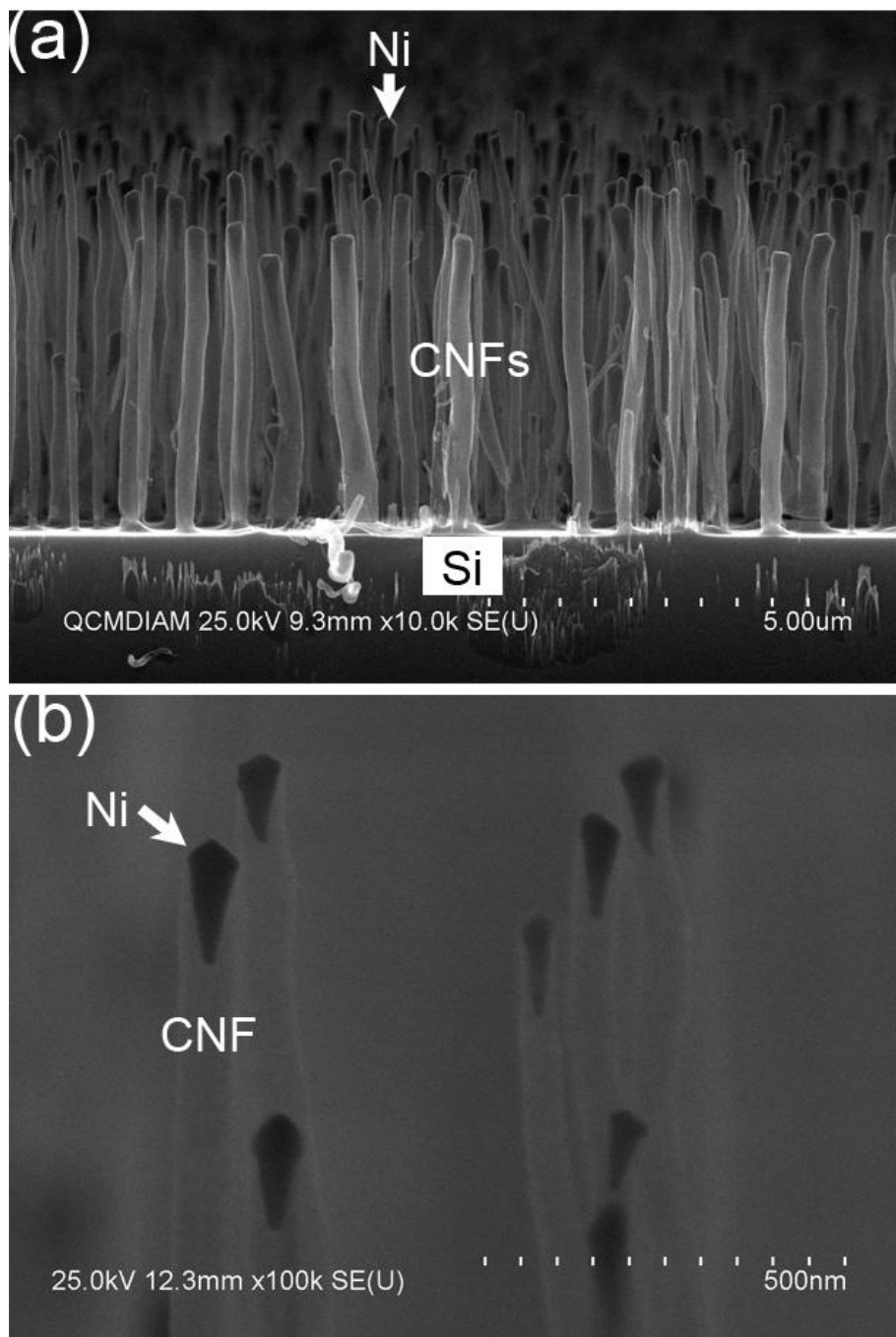


Fig. 1, He *et al.*

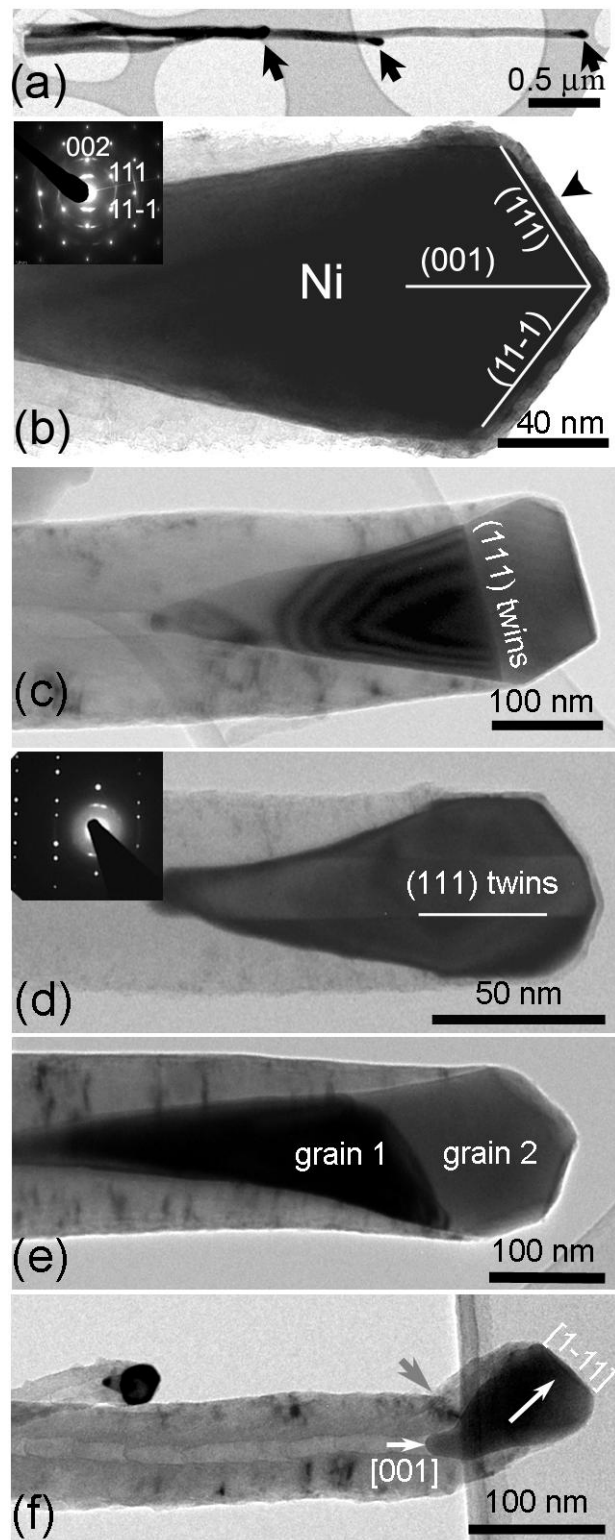


Fig. 2 , He *et al.*

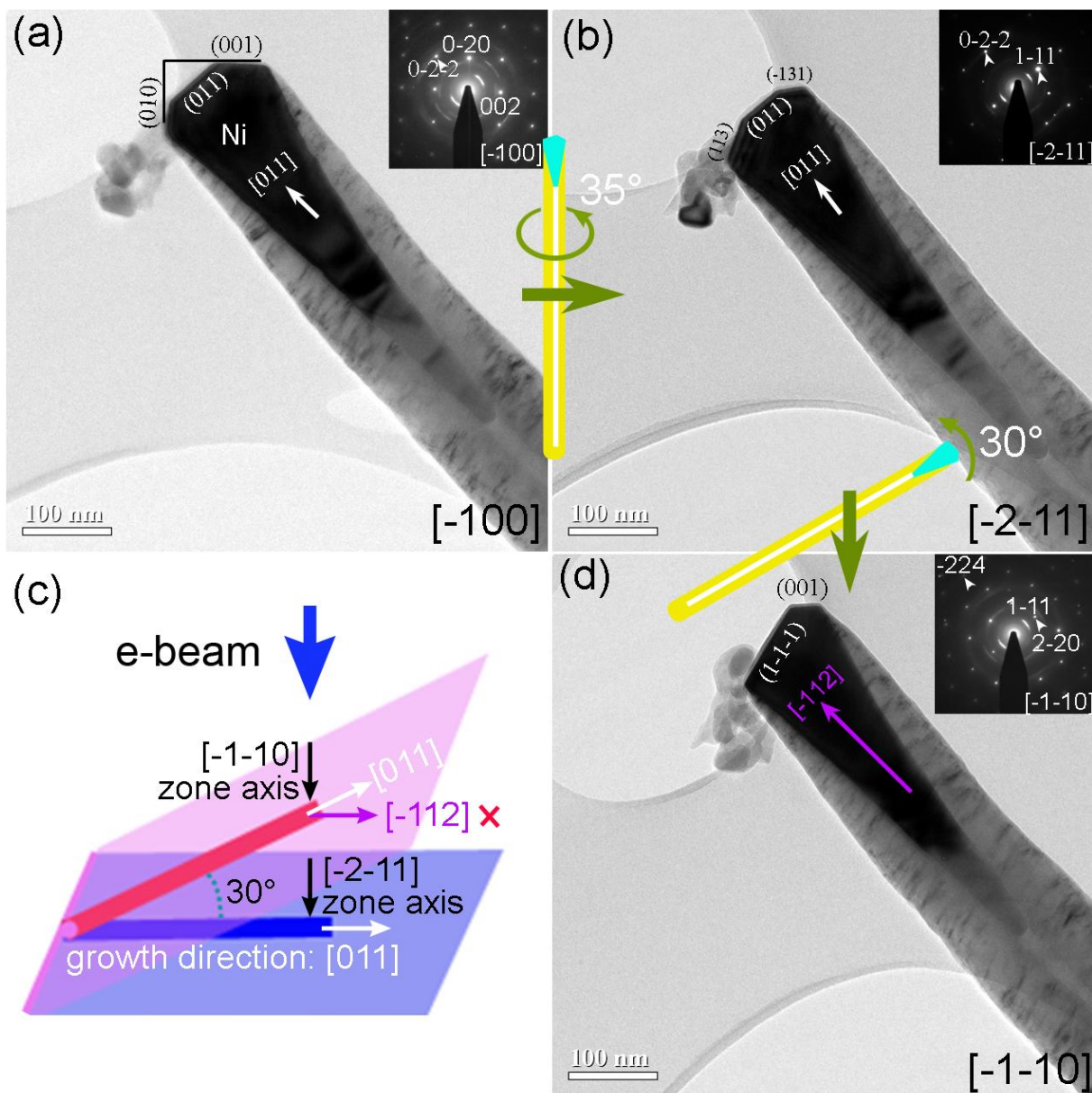


Fig. 3, He *et al.*

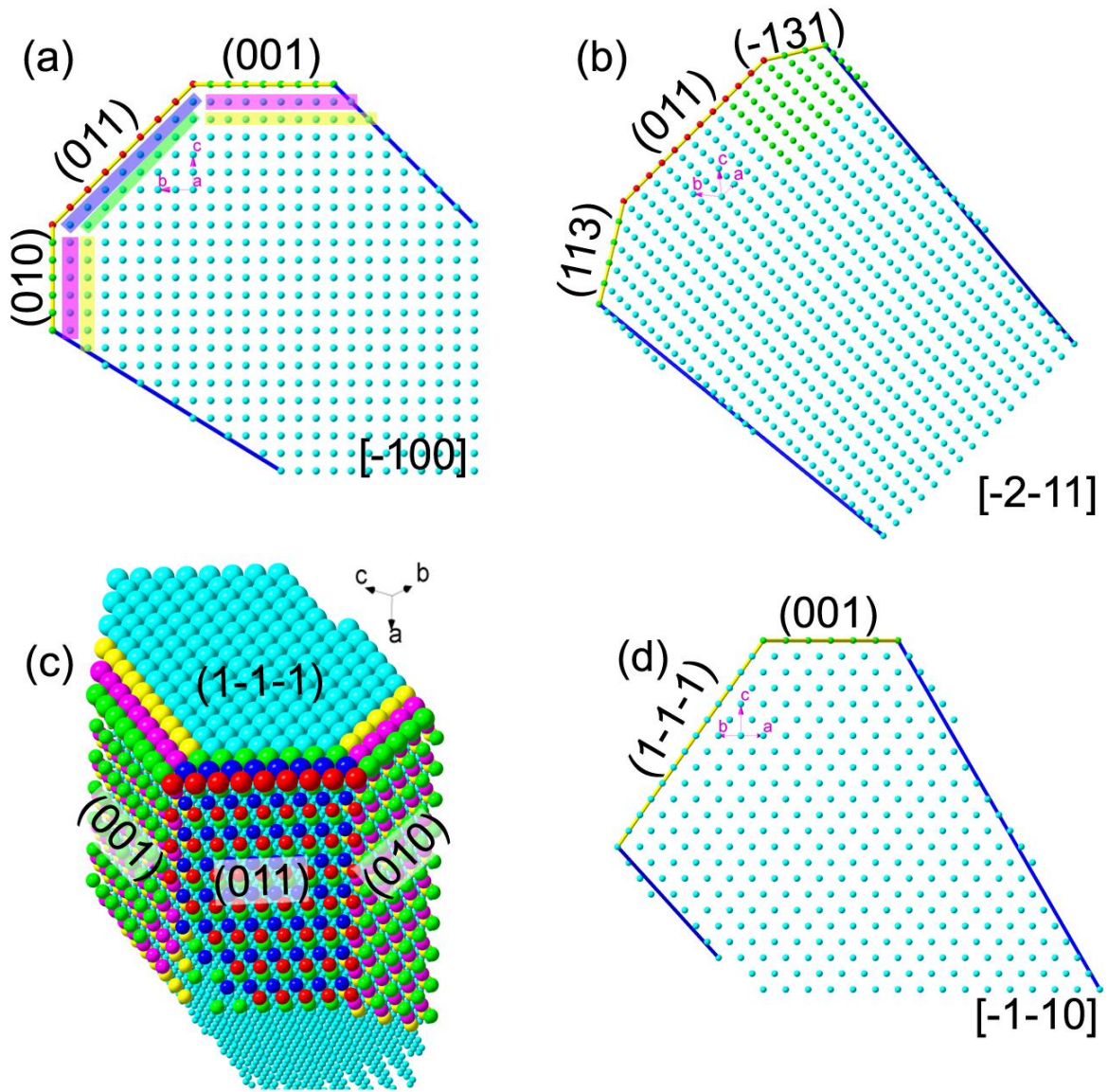


Fig. 4, He *et al.*

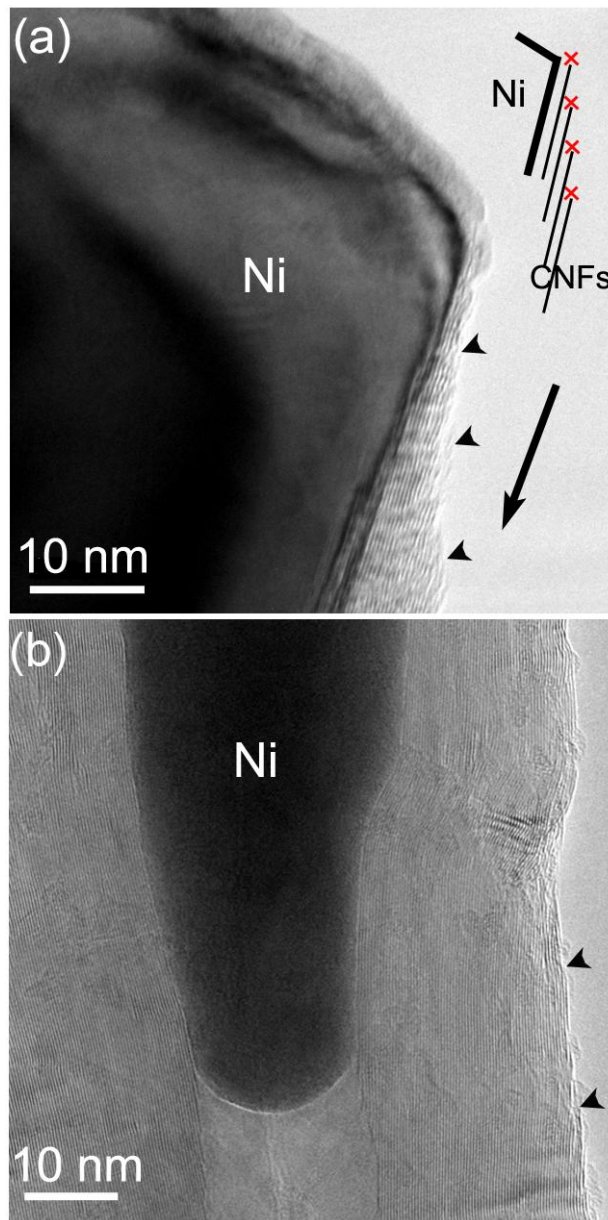


Fig. 5, He *et al.*

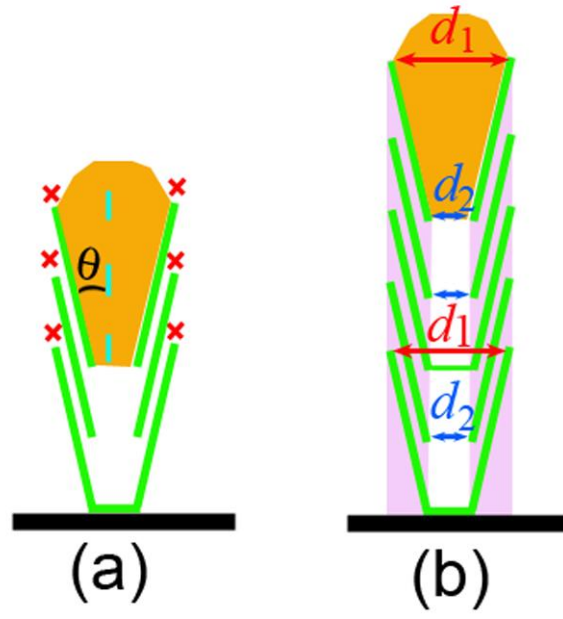


Fig. 6, He *et al.*